Research Square

Preprints are preliminary reports that have not undergone peer review.
They should not be considered conclusive, used to inform clinical practice,
or referenced by the media as validated information.

Phytoplankton eco-physiology enforces nitrogen limitation in the global ocean

Chia-Te Chien

cchien308@ntu.edu.tw

National Taiwan University https://orcid.org/0000-0002-0461-2851

Markus Pahlow

GEOMAR https://orcid.org/0000-0003-2090-5993

S. Lan Smith

JAMSTEC https://orcid.org/0000-0002-2338-5893

Kai Wirtz

Helmholtz Zentrum Heroen, Germany https://orcid.org/0000-0002-6972-3878

Markus Schartau

GEOMAR Helmholtz Centre for Ocean Research Kiel https://orcid.org/0000-0003-1114-0415

Christopher Somes

GEOMAR Helmholtz Centre for Ocean Research Kiel https://orcid.org/0000-0003-2635-7617

Andreas Oschlies

GEOMAR Helmholtz Centre for Ocean Research Kiel https://orcid.org/0000-0002-8295-4013

Article

Keywords:

Posted Date: October 21st, 2026

DOI: https://doi.org/10.21203/rs.3.rs-11010579/v1

License: This work is licensed under a Creative Commons Attribution 4.0 International License.
Read Full License

Additional Declarations: There is **NO** Competing Interest.

Phytoplankton eco-physiology enforces nitrogen limitation in the global ocean

Chia-Te Chien[1], Markus Pahlow[2], Sherwood Lan Smith[3,4,5], Kai W. Wirtz[6,7], Markus Schartau[2], Christopher J. Somes[2], and Andreas Oschlies[2,7]

[1]Institute of Oceanography, National Taiwan University, Taiwan
[2]GEOMAR Helmholtz Centre for Ocean Research Kiel, Kiel, Germany
[3]Advanced Institute for Marine Ecosystem Change [WPI- AIMEC], JAMSTEC, Yokohama, Japan
[4]Advanced Institute for Marine Ecosystem Change [WPI- AIMEC], Tohoku University, Sendai, Japan
[5]Research Institute for Global Change, JAMSTEC, Yokosuka, Japan
[6]Helmholtz-Zentrum Hereon, Geesthacht, Germany
[7]Kiel University, Kiel, Germany

Correspondence: Chia-Te Chien (cchien308@ntu.edu.tw)
Contributing authors: Markus Pahlow (mpahlow@geomar.de); Sherwood Lan Smith (lanimal@jamstec.go.jp); Kai W. Wirtz (kai.wirtz@hereon.de); Markus Schartau (mschartau@geomar.de); Christopher J. Somes (csomes@geomar.de); Andreas Oschlies (aoschlies@geomar.de)

Abstract. The distributions of nutrients essential for autotrophic growth, including nitrogen (N), phosphorus (P), and iron (Fe), largely determine oceanic primary production. According to the homeostasis hypothesis, competition between N_2-fixers and non-N_2-fixers drives the global dissolved N:P ratio (dN:P) to approach that of phytoplankton, thereby stabilising oceanic nutrient ratios [1, 2]. However, flexibility in phytoplankton elemental composition challenges this view, as variable N:P ratios cannot constrain dN:P [3, 4, 5]. We investigate the homeostasis hypothesis by perturbing nutrient inventories in an Earth system model that resolves variable stoichiometry for marine autotrophs. Autotroph stoichiometry adjusts to ambient nutrient ratios in ways that counteract changes in the marine N inventory, generating a strong stabilising feedback. In particular, higher N_2-fixer N:P ratios enhance newly fixed N inputs per unit P assimilated. Our results indicate that increases in P and Fe have surprisingly little impact on long-term primary production because optimal regulation of phytoplankton stoichiometry enforces nitrogen limitation in the modern ocean. These results suggest that phytoplankton eco-physiology can weaken the response of marine productivity and atmospheric CO_2 to nutrient perturbations, with implications for nutrient-based geoengineering and for assessing past or future shifts in elemental cycles.

Key words: homeostasis, variable stoichiometry, primary production, physiology

1 Introduction

In the near-surface ocean the growth of phytoplankton is largely determined by the availability of essential nutrients, in particular the macronutrients nitrogen and phosphorus, along with iron and other micronutrients. Bioavailable nitrogen in the ocean behaves as an open reservoir with biologically mediated exchange between the virtually inexhaustible atmospheric N_2 pool, regulated by spatio-temporal variations in N_2 fixation, nitrification, and denitrification. In contrast, the ocean's

phosphorus reservoir changes on much longer timescales, governed by terrestrial weathering, phosphate influx from land, and redox-sensitive benthic cycling [1, 6]. The horizontal and vertical distribution of oceanic phosphate (PO_4^{3-}) is also much influenced by pelagic biological activity, which in turn is constrained by N_2 fixation and denitrification [6]. These two processes thus produce variable patterns of the dissolved nitrogen-to-phosphorus (dN:P) ratio. Fluctuations in dN:P ultimately reflect competition between N_2-fixers and non-N_2-fixers, while N_2 fixation has been linked to the availability of excess PO_4^{3-}, i.e., $P^* = PO_4^{3-} - NO_3^-/16$ [7, 8].

Oceanic dN:P varies in space and time even under the assumption of fixed elemental stoichiometry for all particulate organic matter (POM), referred to as the Redfield ratio [9, 10]. A constant pN:P imposes a fixed relative biological demand for N and P, providing a reference ratio around which the marine N inventory can be regulated. When dN:P falls below this ratio, excess P favours N_2 fixation and N input; when dN:P rises, denitrification removes N, together driving dN:P toward a characteristic steady-state value [1, 2, 11]. Yet surface pN:P varies widely with nutrient supply through physiological and evolutionary responses [3, 4, 5, 12, 13], challenging this fixed-stoichiometry framework.

Previous studies have taken into account changes in elemental N:P ratios of non-N_2-fixers. For instance, a variable N:P ratio for non-N_2-fixers was proposed to increase excess P (P*), thereby enhancing N_2 fixation to levels sufficient to balance globally observed denitrification and stabilise the nitrogen inventory [14]. Fewer studies have considered the N:P ratio of N_2-fixers, which varies substantially with ${PO_4}^{3-}$ supply in both laboratory experiments and field observations [15, 16, 17, 18, 19, 20, 21], thereby directly determining N_2 fixation relative to phosphorus assimilation [22]. Ultimately, many assumptions underlying marine biogeochemical models therefore remain inconsistent with physiological and biogeochemical observations, particularly regarding interactions among marine N and P cycling and ocean–atmosphere carbon exchange.

Here, we examine global ocean stoichiometric equilibria by explicitly considering physiological fluctuations in the pN:P ratio. To identify key biogeochemical inter-dependencies related to the ocean's N and P pools, we introduce global perturbations to the NO_3^- and PO_4^{3-} and compare the responses of variable- and fixed-stoichiometry model configurations. This allows us to test how flexible phytoplankton elemental ratios modify the constant-stoichiometry framework assumed in previous formulations of the homeostasis hypothesis. We also evaluate the role of Fe supply, which is an essential micronutrient for the growth of both N_2-fixers [23] and non-N_2-fixers [24]. In addition to changes in the dN:P ratio, our sensitivity analyses focus on the associated nitrogen fluxes, export production and atmospheric pCO_2 concentrations. Our model-based analysis shows how the eco-physiological plasticity of marine phytoplankton counterintuitively dampens carbon-sequestration potential, with implications for understanding the robustness of elemental and their shifts across climate states.

2 Results and discussion

2.1 Symmetric restoration following N perturbations vs. asymmetric decoupling after P perturbations

Following N inventory perturbations, dN:P ratios recover on a long time scale, completely converging back to control baselines by year 20k in both fixed-stoichiometry (FS) and variable-stoichiometry (VS) configurations (Fig. 1a). This recovery is closely mirrored by the cellular N:P of non-N_2-fixers and N_2-fixers (Fig. 1c). Atmospheric pCO_2 anomalies (ΔpCO_2) diverge

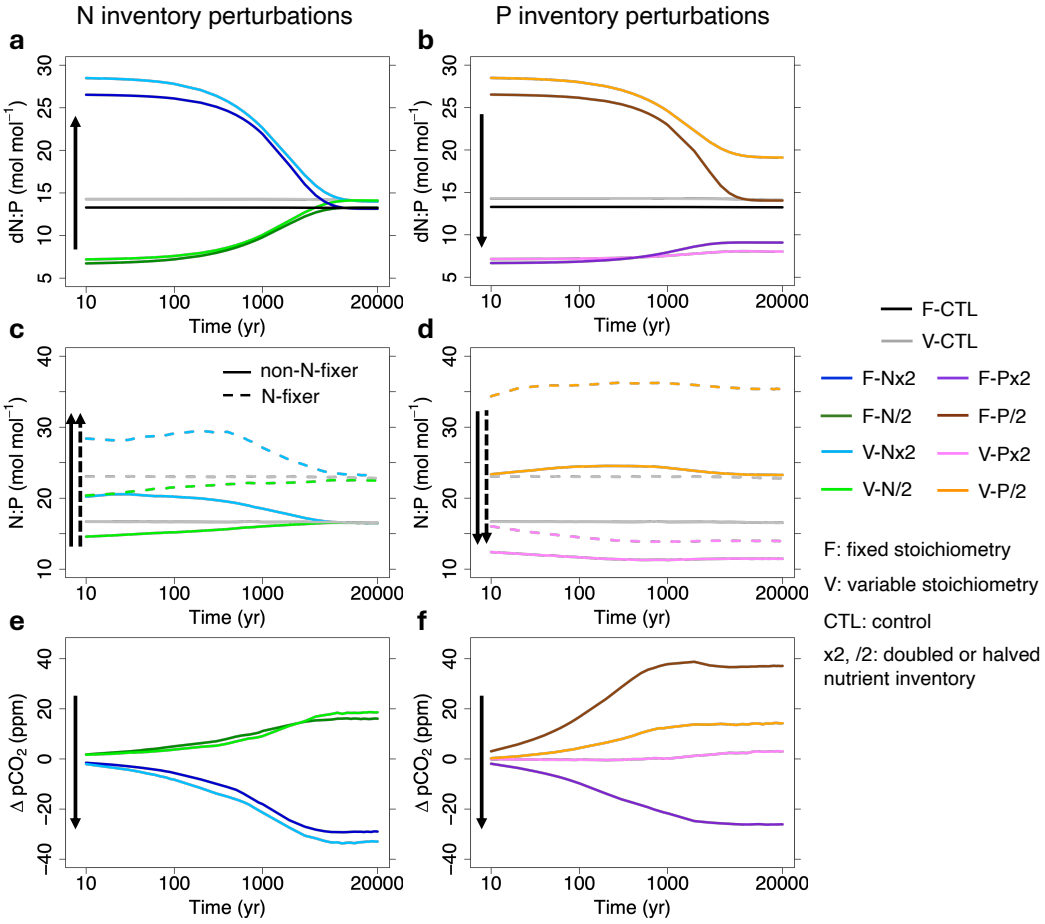

Figure 1. Temporal evolution of marine nutrient stoichiometry and atmospheric pCO_2 in fixed- (FS) and variable-stoichiometry (VS) configurations following NO_3^- or PO_4^{3-} inventory perturbations. **a, b,** Globally averaged dissolved nitrogen to phosphorus ratios (dN:P). **c, d,** N:P ratio shifts in non-N_2-fixers (solid lines) and N_2-fixers (dashed lines). **e, f,** Trajectories of atmospheric pCO_2 anomalies relative to the baseline controls. Black and grey lines represent the FS and VS control simulations, respectively. Vertical arrows indicate the direction of increasing initial nutrient inventories (from halved to doubled) relative to control baselines.

symmetrically early on (Fig. 1e). After year 5k, these pCO_2 anomalies flatten and stabilise, reflecting the re-equilibration of the global N reservoir. The changes in pCO_2 slightly affect surface temperature and the strength of the Atlantic Meridional Overturning Circulation (Extended data Table 1).

By contrast, the regulatory feedbacks are weaker after P perturbations, producing asymmetric responses in which the global climate system enters biogeochemical states that differ from those before the perturbation. Global dN:P ratios remain distinct from their control baselines by year 20k under both the VS and FS assumptions (Fig. 1b). In the FS configuration with halved P inventory (F-P/2), dN:P settles at roughly 6 % higher than in the control, whereas doubling P (F-P×2) drives dN:P to only

69 % of its baseline by year 20k (Fig. 1b, Extended data Table 1). The restoration is even weaker for VS, where the final dN:P reaches 136 % for V-P/2 and drops to 57 % for V-P×2 relative to the control. Reflecting these shifts in dN:P, the N:P ratios of non-N_2-fixers and N_2-fixers mostly retain or amplify their initial deviations from the controls towards the end of the 20k year simulations (Fig. 1d). Notably, atmospheric pCO_2 trends diverge between configurations (Fig. 1f). While the FS configuration yields a substantial pCO_2 drawdown under elevated [PO_4^{3-}] (F-P×2), the VS configuration displays a counterintuitive, albeit weak net increase in atmospheric pCO_2 relative to its baseline control.

Table 1. N_2 fixation and denitrification rates 10 years after NO_3^- perturbation, their differences compared with the control simulations, and the time when NO_3^- concentration has recovered halfway toward the value in year 20k ($T_{50\%}$) of the NO_3 perturbation experiments.

Configuration	Experiment	N_2 fixation	denitrification	ΔN_2 fixation	Δdenitrification	$T_{50\%}$
		(Tmol N year^{-1})				(Year)
VS	V-N×2	2.5	23.9	−12.5 (−83%)	+9.0 (+60%)	1385
	V-N/2	28.8	10.5	+13.7 (+91%)	−4.4 (−30%)	1334
FS	F-N×2	0.3	14.6	−10.4 (−97%)	+3.9 (+37%)	1564
	F-N/2	30.8	9.0	+20.0 (+187%)	−1.7 (−16%)	1105

This divergence in biogeochemically induced climate responses reveals a fundamental difference between the two model configurations: while FS enforces a rigid Redfield ratio (N:P = 16:1) that serves as the baseline for N- and P-limitation, VS produces a global pattern of persistent N-limitation in the surface ocean even if the global P inventory is reduced (Extended data Fig. 1). In the VS baseline, metabolic optimisation allows the N:P ratio of non-N_2-fixers, which dominate total POM, to vary between 8 and 28 (increasing as ambient PO_4^{3-} drops, Extended data Fig. 2). This behaviour is consistent with observations and recent meta-analyses of environmental drivers on phytoplankton stoichiometry [3, 12, 25]. In contrast to the hypothesis that high N:P ratios in non-N_2-fixers indirectly stimulate N_2 fixation by using less PO_4^{3-} in oligotrophic waters [14], our results point to an alternative mechanism driven by the stoichiometric flexibility of N_2-fixers themselves. AS in non-N_2-fixers, the N_2-fixer N:P ratio also increases as ambient [PO_4^{3-}] declines (Extended data Fig. 2). This inverse relationship is well supported by laboratory experiments and field observations [15, 18, 19] (Extended data Fig. 3). Crucially, such intrinsic plasticity allows N_2-fixers to sustain high fixation rates without requiring additional P. While the N_2 fixation rates in both FS and VS configurations fall within global estimates of $9.0 - 15.9$ Tmol N year^{-1} [26], P assimilation by N_2-fixers in VS is 9% lower than in FS. In contrast, global N_2 fixation is 41 % higher in VS, owing to the 44 % higher N:P ratio of N_2-fixers (Extended data Table 2). Thus, the essential difference is that N_2-fixer stoichiometric flexibility in VS decouples N_2 fixation from P supply, weakening the sensitivity of marine N input to changes in nutrient inventories.

The rapid restoration of global dN:P and atmospheric pCO_2 following N perturbations is driven by compensatory shifts in marine N_2 fixation and denitrification (Fig. 2a). Altered competition between N_2-fixers and non-N_2-fixers creates strong regulatory feedbacks that spatially reorganise N_2-fixation and denitrification to a similar degree for both VS and FS. At equilibrium, the sources and sinks of bioavailable N adjust, thereby counteracting the inventory changes: in simulations with

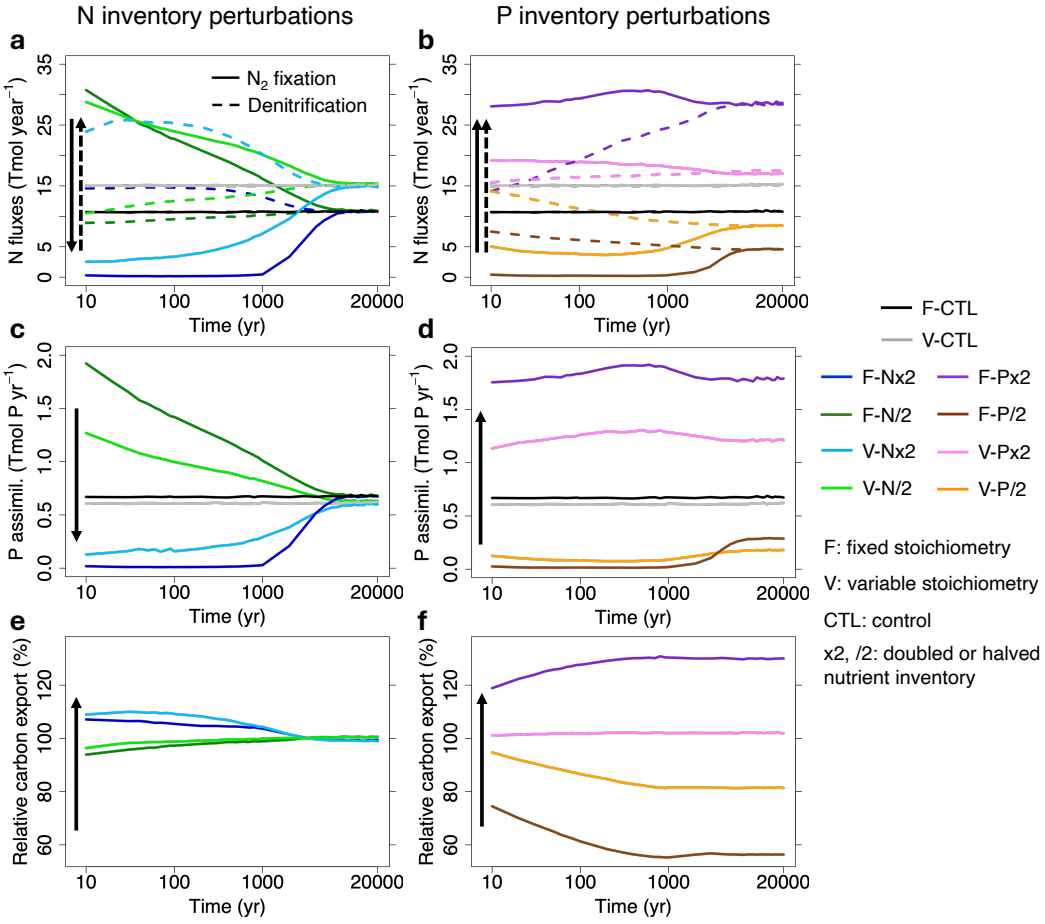

Figure 2. Temporal evolution of nitrogen fluxes, P assimilation, and POC export in fixed- (FS) and variable-stoichiometry (VS) configurations following NO_3^- or PO_4^{3-} inventory perturbations. **a, b,** Global N_2 fixation (solid lines) and denitrification (water-column and benthic denitrification, dashed lines). **c, d,** Global phosphorus assimilation by N_2-fixers. **e, f,** Trajectories of global carbon export anomalies relative to the baseline controls. Black and grey lines represent the FS and VS control simulations, respectively. Vertical arrows indicate the direction of increasing initial nutrient inventories (from halved to doubled) relative to control baselines.

higher initial NO_3^-, N_2 fixation decreases while denitrification increases; conversely, in simulations with lower initial NO_3^-, N_2 fixation increases while denitrification decreases. This regulatory feedback is a crucial mechanism for restoring dN:P for both VS and FS, in agreement with previously proposed nutrient-homeostasis hypothesis [1, 2, 11], although the recovery timescales differ among the perturbation experiments (Table 1).

The time course of the re-balancing reveals a major divergence between VS and FS driven by eco-physiology. Within ten years after doubling the N inventories (F-N×2 and V-N×2), denitrification increases by 60 % in the VS configuration and 37 % in FS, whereas the decline after halving the N inventory is much smaller because the surface ocean was already N-limited

(Table 1 and Fig. 2a). Simultaneously, N_2 fixation collapses completely for over 1,000 years for F-N×2 but gradually recovers along a smooth trajectory in V-N×2. After nitrogen reduction (N/2), global N_2 fixation increases by 187 % in the FS model versus a more moderate 91 % increase in the VS model.

When NO_3^- is halved, intense N-limitation reduces PO_4^{3-} uptake by non-N_2-fixers, particularly in FS. Consequently, P assimilation by N_2-fixers increases far more in the FS (Fig. 2c), accompanied by a larger increase in N_2 fixation in FS than in VS. This asymmetry renders recovery faster in VS than in FS after an increase in NO_3^-, but slower after a decrease in NO_3^- (Table 1). Similar to dN:P, carbon export mostly recovers towards the original values after year 5,000 (Fig. 2e).

Beyond merely capturing present-day observations, the VS configuration offers a general explanation for persistent N-limitation in the World Ocean [27] as a consequence of metabolic optimisation. After doubling the N inventory, the global N:P of POM increases from 16.7 to $19.4\,\mathrm{mol\,mol^{-1}}$, accelerating NO_3^- utilisation and restoring N limitation (Fig. 3a). While a related stabilising feedback has been identified in previous fixed-composition Earth system models under anthropogenic nitrogen loads (Supplementary Discussion), variable stoichiometry strengthens this feedback by increasing cellular N:P, thereby accelerating N drawdown relative to P (Fig. 3a,c). When PO_4^{3-} is halved, the N:P of POM rises to $21.8\,\mathrm{mol\,mol^{-1}}$ in VS, which helps maintain a N-limited ocean (Fig. 3c). In contrast, the FS configuration quickly runs into P limitation after perturbations in F-N×2 and F-P/2 (Fig. 3b,d).

Simulated N_2 fixation and denitrification mostly vary inversely under NO_3^- manipulations, responses to PO_4^{3-} manipulations occur sequentially, whereby changes in N_2 fixation precede and drive subsequent changes in denitrification (Fig. 2b). This is contrary to the assumption that N_2 fixation merely "tops-up" the N deficit caused by denitrification [7].

Doubling the PO_4^{3-} inventory increases global N_2 fixation by 166% in FS but only by 11% in VS at year 20k (Fig. 2b). This muted response in VS arises primarily from flexibility in the N:P ratio of N_2-fixers, which determines N_2 fixation relative to assimilated P. Their N:P ratio declines as $[PO_4^{3-}]$ increases (Extended data Fig. 2b), falling from $22.8\,\mathrm{mol\,mol^{-1}}$ in the control to $14.0\,\mathrm{mol\,mol^{-1}}$ at year 20k in V-P×2 (Fig. 1d). This explains the relative insensitivity of N_2 fixation to $[PO_4^{3-}]$ even when P assimilation almost doubles (Fig. 2d). For the same reason, N_2 fixation decreases less in VS than in FS (44% vs 57%) in the P/2 simulations (Fig. 2b). Thus, variable N_2-fixer stoichiometry buffers PO_4^{3-} perturbations by reducing the sensitivity of N_2 fixation, stabilising the marine nitrogen inventory and weakening the response of export production relative to FS (Fig. 2f).

At year 20k, V-P×2 shows only small changes in export production and atmospheric pCO_2; export increases slightly while atmospheric pCO_2 remains above the control (Fig. 1f and 2f), in stark contrast to the low pCO_2 obtained with the FS configuration. The enhanced export production is concentrated primarily in low-latitude oligotrophic regions, whereas air–sea carbon flux decreases in the North Atlantic, a region that plays a disproportionate role in long-term carbon sequestration (Extended data Fig. 4). This redistribution reduces the efficiency with which biologically fixed carbon is transferred to the deep ocean, offsetting the effect of higher global export production and resulting in a weak net increase in atmospheric pCO_2.

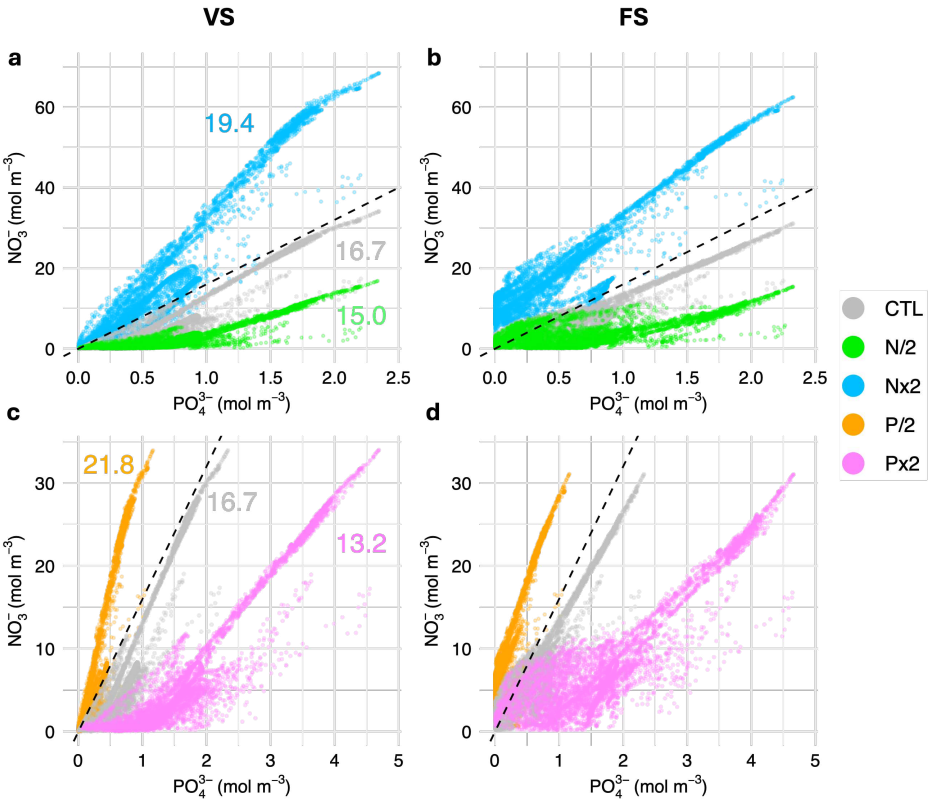

Figure 3. Surface (0 to 50 m) NO_3^- versus PO_4^{3-} concentrations 10 years after nutrient inventory modifications. a, b, Control, N/2, and N×2 modifications under (a) variable (VS) and (b) fixed stoichiometry (FS) configurations. c, d, Control, P/2, and P×2 modifications under (c) variable and (d) fixed stoichiometry configurations. Coloured numbers denote global median surface particulate N:P ratios. Dashed lines indicate a 16:1 NO_3^-:PO_4^{3-} ratio and intercept at the origin.

2.2 Auto-regulation of plankton ecology and ocean biogeochemistry

Our results challenge the traditional distinction between 'proximate' N and 'ultimate' P limitation [1], indicating that the ocean remains fundamentally N-limited on both short and long timescales. The ratio of N and P assimilation imposed by the optimal regulation in UVic-OPEM is a strong function of the ratio of the N and P subsistence quotas [28, 29, 30] and far exceeds oceanic dN:P ratios for commonly observed subsistence quotas [28]. Thus, simulated pN:P ratios remain consistently greater than dN:P, aligning well with field observations (Fig. 4). This elevated biological ratio reflects a net nutrient uptake that exceeds ambient dissolved proportions, tightening the surface ocean into an N-limited state. The persistent N-limitation, however, governs global carrying capacity through an asymmetric threshold. Under halved phosphorus (P/2), global productivity and carbon export drop significantly because the ecosystem hits a hard physiological limit; stoichiometric flexibility can only conserve P up to a structural limit, as cells require a baseline concentration for essential metabolic machinery (e.g., ribosomal RNA).

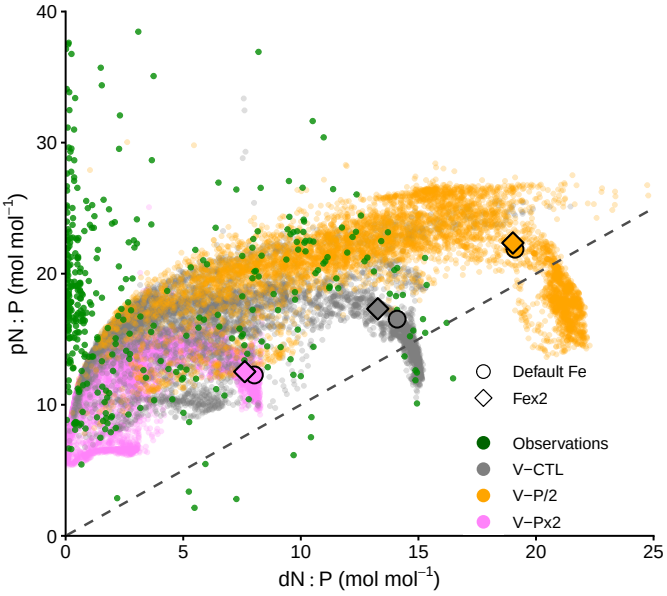

Figure 4. Nitrogen:Phosphorus ratio of particulate organic matter (pN:P) versus dissolved inorganic matter (dN:P) in the surface (0 to 50 m) in observations [12, 33] and in the V-CTL, V-P/2, and V-P×2 simulations. Large symbols denote global medians of the surface pN:P versus globally averaged dN:P in experiments with default and doubled Fe deposition (Fe×2). The dashed line indicates a 1:1 ratio.

Conversely, under doubled phosphorus (P×2), production hits a regulatory ceiling enforced by the N:P flexibility of N_2-fixers. By lowering their cellular N:P requirements rather than boosting absolute fixation rates, N_2-fixers satisfy their own growth without expanding the global NO_3^- inventory in full Redfield proportion to the augmented PO_4^{3-} inventory. The broader non-N_2-fixer community therefore remains constrained by persistent nitrogen depletion. This asymmetric response implies that the contemporary marine ecosystem already operates at near-optimal efficiency relative to the ambient phosphorus supply, positioned precisely at the interface of structural limitation and regulatory saturation.

While traditional paradigms suggest that pN:P largely determines dN:P [1, 2, 8, 31, 32], our PO_4^{3-} perturbation experiments reveal bidirectional coupling: nutrient availability alters phytoplankton stoichiometry, which in turn modifies N cycling and nutrient inventories (Fig. 4). This relationship persists under doubled Fe deposition because Fe-stimulated N_2 fixation is offset by enhanced export and denitrification (Fe×2, Supplementary Discussion and Extended data Figs. 5 and 6). The strong dependence of pN:P on the phytoplankton subsistence quotas suggests that the key to comprehending oceanic macro-nutrient biogeochemistry could lie in understanding the (evolutionary) drivers of these subsistence quotas.

Consistent with other observation-based results (Supplementary Discussion), our results suggest that long-term changes in dN:P need not arise solely from changes in species composition [34]. Physiological acclimation to changing ambient nutrient ratios can itself substantially alter pN:P and, by modifying N cycling, influence dN:P over timescales from decades to millennia. This does not exclude an important role for community composition, particularly if subsistence quotas covary with species traits such as cell size, in which case shifts in community composition could modify the aggregate stoichiometric response. Our

results also reveal remaining challenges, including the mutual interdependence between dN:P and pN:P identified herein and the seeming paradox that physiological plasticity [4, 13] tends to enforce N limitation in our model. This eco-physiological buffering may constrain the response of marine productivity and atmospheric CO_2 to natural or anthropogenic changes in nutrient supply, with implications for interpreting past shifts in elemental cycles and assessing the effectiveness of nutrient-based geoengineering.

Declarations

Funding

Chia-Te Chien is supported by Taiwan National Science and Technology Council grants NSTC 115-2611-M-002-004-.

Availability of code and data

Model codes and outputs used for the experiments and analyses are available at https://doi.org/10.5281/zenodo.22076944.

Author contributions

C.-T.C. conceived and designed the study. C.-T.C. conducted the UVic-OPEM simulations, performed the data analysis, and wrote the initial draft of the manuscript. M.P. contributed to the development and implementation of the optimality-based ecosystem model formulations. All authors (C.-T.C., M.P., S.L.S., K.W.W., M.S., C.J.S., and A.O.) contributed to the interpretation of the model results, discussed the underlying ecological and biogeochemical mechanisms, and critically reviewed and edited the manuscript.

Competing interests

The authors declare no competing interests.

Acknowledgments

The authors acknowledge NOAA's Pacific Marine Environmental Laboratory for the Ferret program, the R Core Team, and the developers of ggplot2 for the open-source software used for analysis and visualisation.

Methods

Fixed and variable elemental stoichiometry model for particulate organic matter

We use an optimality-based non-Redfield ecosystem model embedded into a 3D Earth system climate model, UVic-OPEM [29, 30]. Elemental ratios (carbon:nitrogen:phosphorus) of non-N_2-fixers, N_2-fixers, and detritus in UVic-OPEM vary with environmental conditions, whereas a fixed C:N:P ratio is applied for zooplankton. The variable-stoichiometry formulation has been extensively tested using laboratory and field data [28, 29]. To compare the effects of fixed and variable stoichiometry, we have developed a fixed-stoichiometry version of the UVic-OPEM. The original (variable-stoichiometry) version of UVic-OPEM is referred to as the VS configuration and the fixed-stoichiometry version as the FS configuration.

In the optimality-based model, nutrient limitation is formulated as a chain model [28]: Carbon fixation (V^{C}) is limited by the cellular nitrogen quota ($Q^{\mathrm{N}} = $ N:C ratio), and nitrogen acquisition is limited by the phosphorus quota ($Q^{\mathrm{P}} = $ P:C ratio). Nitrogen acquisition is either DIN (dissolved inorganic nitrogen) uptake (V^{N}) or N_2 fixation (F^{N}). Both V^{N} and phosphorus uptake (V^{P}) follow optimal uptake kinetics. The nitrogen quota is divided into three parts, (1) a fixed (non-allocatable) partial quota $Q_{\mathrm{s}}^{\mathrm{N}}$, representing structural protein, (2) fraction f_{V}, allocated to nutrient uptake and assimilation in the protoplast, and (3) fraction $f_{\mathrm{C}} = 1 - Q_{\mathrm{s}}^{\mathrm{N}}/Q^{\mathrm{N}} - f_{\mathrm{V}}$ for carbon (C) fixation in the chloroplast. Fraction f_{V} is subdivided between N uptake ($f_{\mathrm{V}} \cdot f_{\mathrm{N}}$) and P uptake ($f_{\mathrm{V}} \cdot (1 - f_{\mathrm{N}})$). The allocation factors (variable fractions) f_{V} and f_{N} relate actual (V^{C}, V^{N}, F^{N}, V^{P}) to potential specific rates ($\widehat{V}^{\mathrm{C}}$, $\widehat{V}^{\mathrm{N}}$, $\widehat{F}^{\mathrm{N}}$, $\widehat{V}^{\mathrm{P}}$) of C fixation and nutrient acquisition:

$$ {}^{\mathrm{VS}}V^{\mathrm{C}} = ({}^{\mathrm{VS}}f_{\mathrm{C}} \cdot \widehat{V}^{\mathrm{C}} - R) \cdot C \tag{1} $$

$$ {}^{\mathrm{VS}}V^{\mathrm{N}} = {}^{\mathrm{VS}}f_{\mathrm{V}} \cdot {}^{\mathrm{VS}}f_{\mathrm{N}} \cdot {}^{\mathrm{VS}}\widehat{V}^{\mathrm{N}} \cdot C \tag{2} $$

$$ {}^{\mathrm{VS}}F^{\mathrm{N}} = {}^{\mathrm{VS}}f_{\mathrm{V}} \cdot {}^{\mathrm{VS}}f_{\mathrm{N}} \cdot {}^{\mathrm{VS}}\widehat{F}^{\mathrm{N}} \cdot C \tag{3} $$

$$ {}^{\mathrm{VS}}V^{\mathrm{P}} = {}^{\mathrm{VS}}f_{\mathrm{V}} \cdot (1 - {}^{\mathrm{VS}}f_{\mathrm{N}}) \cdot \widehat{V}^{\mathrm{P}} \cdot C \tag{4} $$

where the left-superscript $^{\mathrm{VS}}$ indicates variables specific to the VS configuration, R is the respiration cost of biosynthesis (the cost of photosynthesis is subsumed in $\widehat{V}^{\mathrm{C}}$) and C the biomass concentration of phytoplankton, used here to convert the specific rates in mol mol $\mathrm{C}^{-1}\mathrm{d}^{-1}$ to absolute rates in mmol $\mathrm{m}^{-3}\mathrm{d}^{-1}$. N_2 fixers are considered facultative diazotrophs in UVic-OPEM, which switch between DIN uptake and N_2 fixation depending on the ambient conditions, but only one of V^{N} and F^{N} can be non-zero at any point in time.

Definitions and expressions of all terms in (1) to (4) and their derivations are provided in the Supplementary Methods and Extended data Table 3. The optimal solutions for the allocation factors f_{V} and f_{N} are defined for the VS configuration in terms of the N and P quotas Q^{N} and Q^{P}, which contain integrated information about nutrient and light conditions of the past couple of days.

Since the quotas are constant in the FS configuration, and hence contain no information about the ambient conditions, we redefine the allocation factors in terms of balanced-growth equivalents of the VS expressions (Supplementary Methods) to obtain solutions as close as possible to an optimal regulation. Nevertheless, maximal growth is achieved only as long as the

fixed values for Q^{N} and Q^{P} happen to be close to the actual optimal values as determined by the allocation factors in the VS configuration. Therefore, the constant Q^{N} and Q^{P} quotas in the FS configuration are incompatible with truly optimal growth.

The FS configuration lacks tracers for phytoplankton particulate organic C and P. Thus, C and N_2 fixation and nutrient uptake are restricted according to a Blackman formula in order to maintain mass balance:

$$V^{\mathrm{C}} = \min\left[{}^{\mathrm{FS}}f_{\mathrm{C}} \cdot \widehat{V}^{\mathrm{C}} - R, \quad {}^{\mathrm{FS}}f_{\mathrm{V}} \cdot {}^{\mathrm{FS}}f_{\mathrm{N}} \cdot \frac{{}^{\mathrm{FS}}\widehat{V}^{\mathrm{N}} + {}^{\mathrm{FS}}\widehat{F}^{\mathrm{N}}}{Q^{\mathrm{N}}}\right] \cdot C, \qquad {}^{\mathrm{FS}}f_{\mathrm{C}} = 1 - \frac{Q_{\mathrm{s}}^{\mathrm{N}}}{Q^{\mathrm{N}}} - {}^{\mathrm{FS}}f_{\mathrm{V}} \tag{5}$$

and the net rates for the FS configuration of N uptake (${}^{\mathrm{FS}}V^{N}$) or N_2 fixation (${}^{\mathrm{FS}}F^{\mathrm{N}}$) and P uptake (${}^{\mathrm{FS}}V^{P}$) are

$${}^{\mathrm{FS}}V^{\mathrm{N}} = {}^{\mathrm{FS}}V^{\mathrm{C}} \cdot Q^{\mathrm{N}} \cdot \frac{{}^{\mathrm{FS}}\widehat{V}^{\mathrm{N}}}{{}^{\mathrm{FS}}\widehat{V}^{\mathrm{N}} + {}^{\mathrm{FS}}\widehat{F}^{\mathrm{N}}} \tag{6}$$

$${}^{\mathrm{FS}}F^{\mathrm{N}} = {}^{\mathrm{FS}}V^{\mathrm{C}} \cdot Q^{\mathrm{N}} \cdot \frac{{}^{\mathrm{FS}}\widehat{F}^{\mathrm{N}}}{{}^{\mathrm{FS}}\widehat{V}^{\mathrm{N}} + {}^{\mathrm{FS}}\widehat{F}^{\mathrm{N}}} \tag{7}$$

$${}^{\mathrm{FS}}V^{\mathrm{P}} = {}^{\mathrm{FS}}V^{\mathrm{C}} \cdot Q^{\mathrm{P}} \tag{8}$$

where, again, only one of ${}^{\mathrm{FS}}V^{\mathrm{N}}$ or ${}^{\mathrm{FS}}F^{\mathrm{N}}$ can be non-zero at any one time. All definitions, expressions and their derivations from the VS configuration in (5) to (8) are provided in the Supplementary Methods and Extended data Table 3. Further, we apply a constant half-saturation iron concentration for the effects of iron limitation on ${}^{\mathrm{FS}}V^{C}$, ${}^{\mathrm{FS}}V^{N}$, and ${}^{\mathrm{FS}}F^{N}$.

Model experiments with perturbed global nitrate and phosphate inventories

A simulation with fixed stoichiometry was restarted from a calibrated simulation with variable stoichiometry, and both simulations were spun up for over 10,000 years with a prescribed pre-industrial atmospheric pCO_2 of 284.3 ppm. A suite of model experiments is examined here, based on variable- (VS) and fixed-stoichiometry (FS; C:N:P = 106:16:1) model configurations, each starting from the steady-state solution of its corresponding spin-up simulation with constant atmospheric pCO_2. Simulations ran over 20k years with a freely evolving atmospheric pCO_2 and climate.

For both model configurations, total nitrogen and phosphorus pools were perturbed within four setups, in which the global pool of NO_3^- or PO_4^{3-} was either halved or doubled relative to the VS and FS controls. Each of these inventory perturbation setups has been complemented by simulations that include a twofold increase in global Fe deposition. Together with the four control runs (variable and fixed stoichiometry with and without doubled Fe deposition), a total set of twenty model experiments is available for evaluation and comparison (Table 2).

N_2 fixation is facultative in the Optimality-based Ecosystem Model (OPEM) [28]. To isolate active N_2-fixers when calculating their N:P ratios and phosphorus assimilation in the VS configuration, we exclude grid cells where the N_2 fixation rate is below $1\,\mu\mathrm{mol\,m^{-3}\,day^{-1}}$. In the VS spun-up simulation, the global N_2 fixation rate is $15.0\ \mathrm{Tmol\,year^{-1}}$. Total nitrogen acquisition by diazotrophs, including both DIN assimilation and N_2 fixation, is $30.6\ \mathrm{Tmol\,year^{-1}}$ before applying the threshold. After applying the N_2-fixation threshold, the total nitrogen acquisition associated with active N_2-fixing grid cells is reduced to $14.9\ \mathrm{Tmol\,year^{-1}}$. Thus, the threshold removes diazotrophs nitrogen acquisition occurring in grid cells with negligible N_2 fixation, allowing the N:P ratios and phosphorus assimilation of active N_2-fixers to be diagnosed more specifically. This

Table 2. Nutrient perturbation experiments with variable (VS) and fixed stoichiometry (FS).

Configuration	Fe deposition	control	NO_3^- inventory		PO_4^{3-} inventory	
			$\div 2$	$\times 2$	$\div 2$	$\times 2$
VS	default	V-CTL	V-N/2	V-N$\times$2	V-P/2	V-P$\times$2
	doubled	V-Fe$\times$2-CTL	V-Fe$\times$2-N/2	V-Fe$\times$2-N$\times$2	V-Fe$\times$2-P/2	V-Fe$\times$2-P$\times$2
FS	default	F-CTL	F-N/2	F-N$\times$2	F-P/2	F-P$\times$2
	doubled	F-Fe$\times$2-CTL	F-Fe$\times$2-N/2	F-Fe$\times$2-N$\times$2	F-Fe$\times$2-P/2	F-Fe$\times$2-P$\times$2

filtering is therefore used only for diagnosing active N_2-fixer stoichiometry and phosphorus assimilation, not for redefining the global N_2 fixation rate.

Given the lack of sources and sinks for oceanic phosphorus in the model, modifications in the PO_4^{3-} inventory permanently change the PO_4^{3-} supply to the upper ocean. For P$\times$2, the increased supply to the surface can be viewed as fertilisation with PO_4^{3-} compared to the standard configuration.

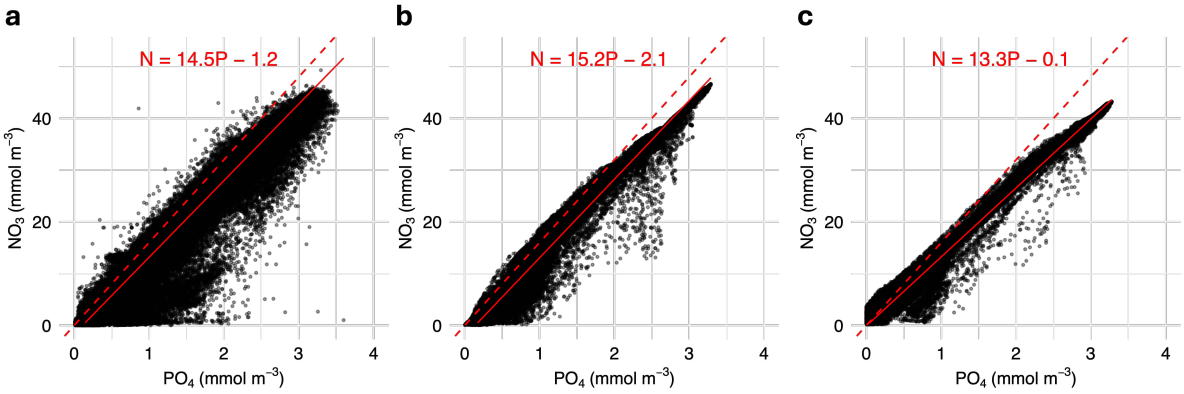

Figure 1. NO_3^-: PO_4^{3-} in observations and in the control simulations at the 10th year. a, World Ocean Atlas. b, c, Simulations with (b) variable and (c) fixed stoichiometry configurations. World Ocean Atlas data were randomly subsampled to 10% of the original size for visualisation. Dashed lines indicate a 16:1 NO_3^-:PO_4^{3-} ratio and intercept at the origin. Solid fitting lines are calculated using the function *lm* (Fitting Linear Models) in the software 'R'.

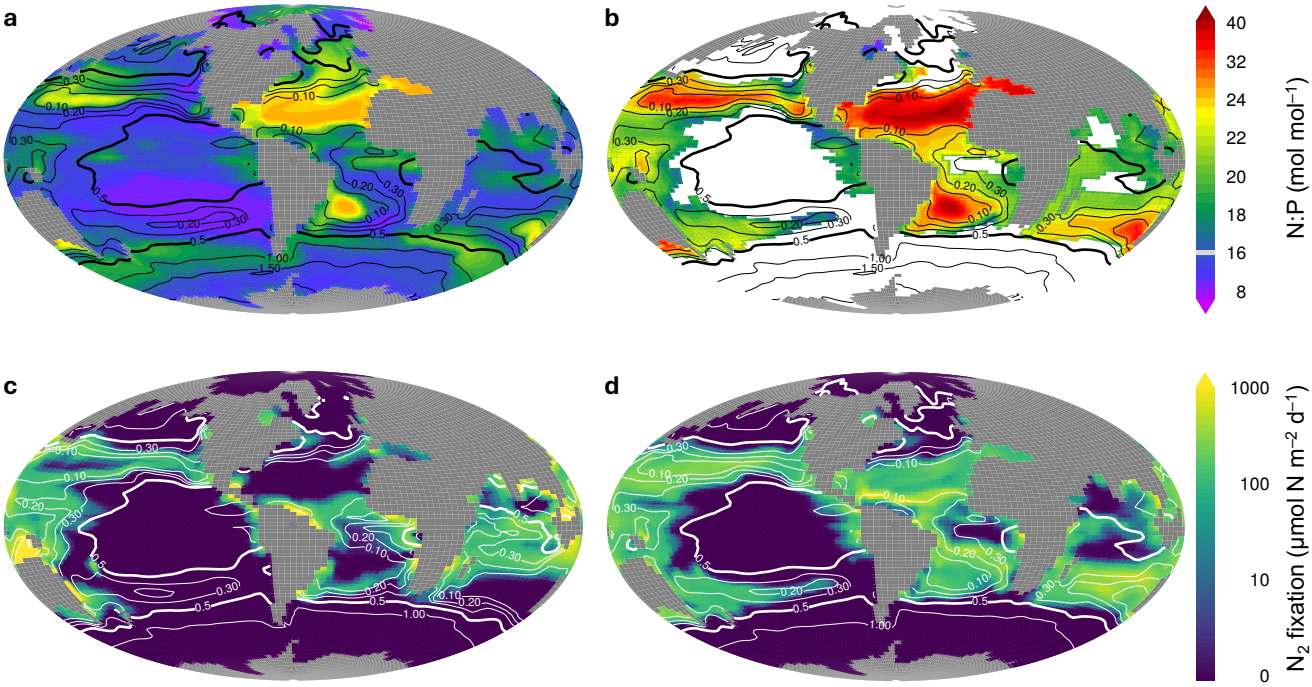

Figure 2. Elemental ratios and N_2 fixation at 10th year in the control simulations. a, b, N:P ratio of non-N_2-fixers (a) and N_2-fixers (b) in the variable stoichiometry control simulation. c, d, N_2 fixation in fixed (c) and variable stoichiometry (d) control simulations. Black and white contour lines indicate surface PO_4^{3-} concentrations of 0.1, 0.2, 0.3, 0.5, and 1 mmol m^{-3}. The grey line in the elemental ratio color bar denotes N:P ratios 16 for the non-N_2-fixers and N_2-fixers in the fixed-stoichiometry configuration.

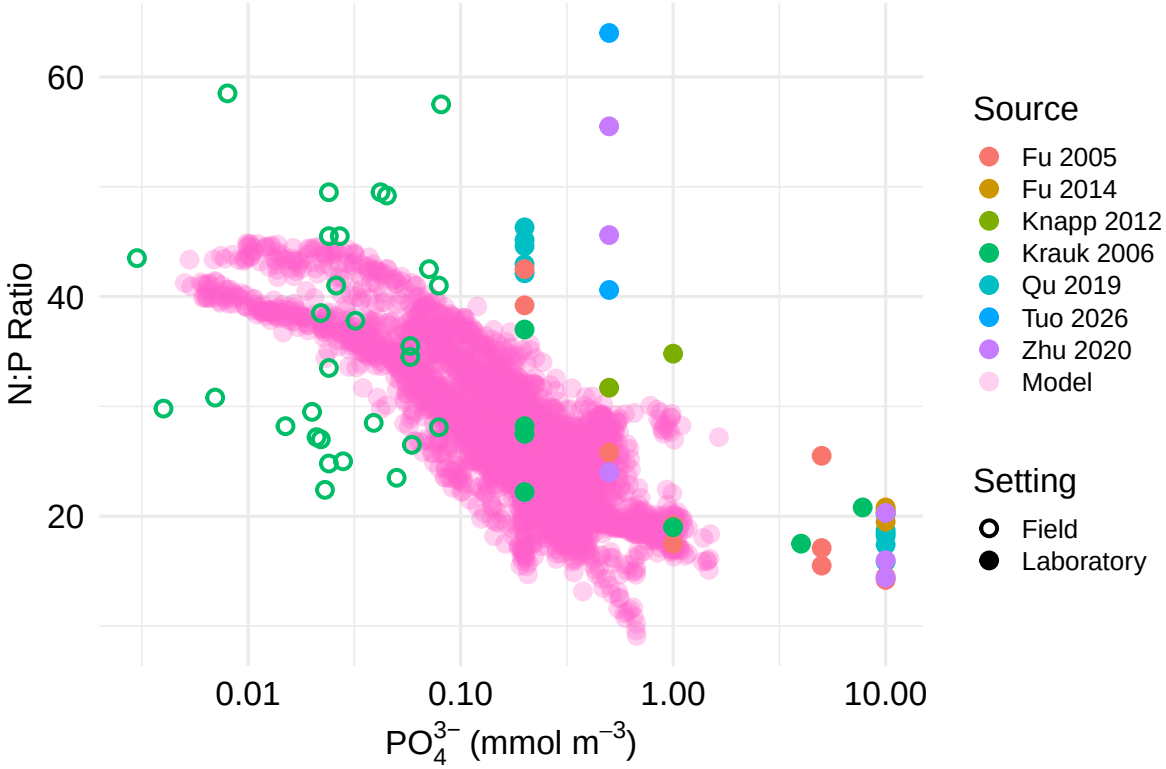

Figure 3. N_2-fixer N:P ratios versus ambient PO_4^{3-} concentrations in field observations, laboratory batch experiments, and in the VS control model results. Fu 2005, Fu 2014, Knapp 2012, Krauk 2006, Qu 2019, Tuo 2026, and Zhu 2020 stand for [15], [16], [17], [18], [19], [20], and [21], respectively. For the laboratory batch experiments, PO_4^{3-} values are the initial concentrations of the culture medium, except for Krauk 2006, for which PO_4^{3-} samples were collected concurrently with the samples used to determine N_2-fixer N:P ratios.

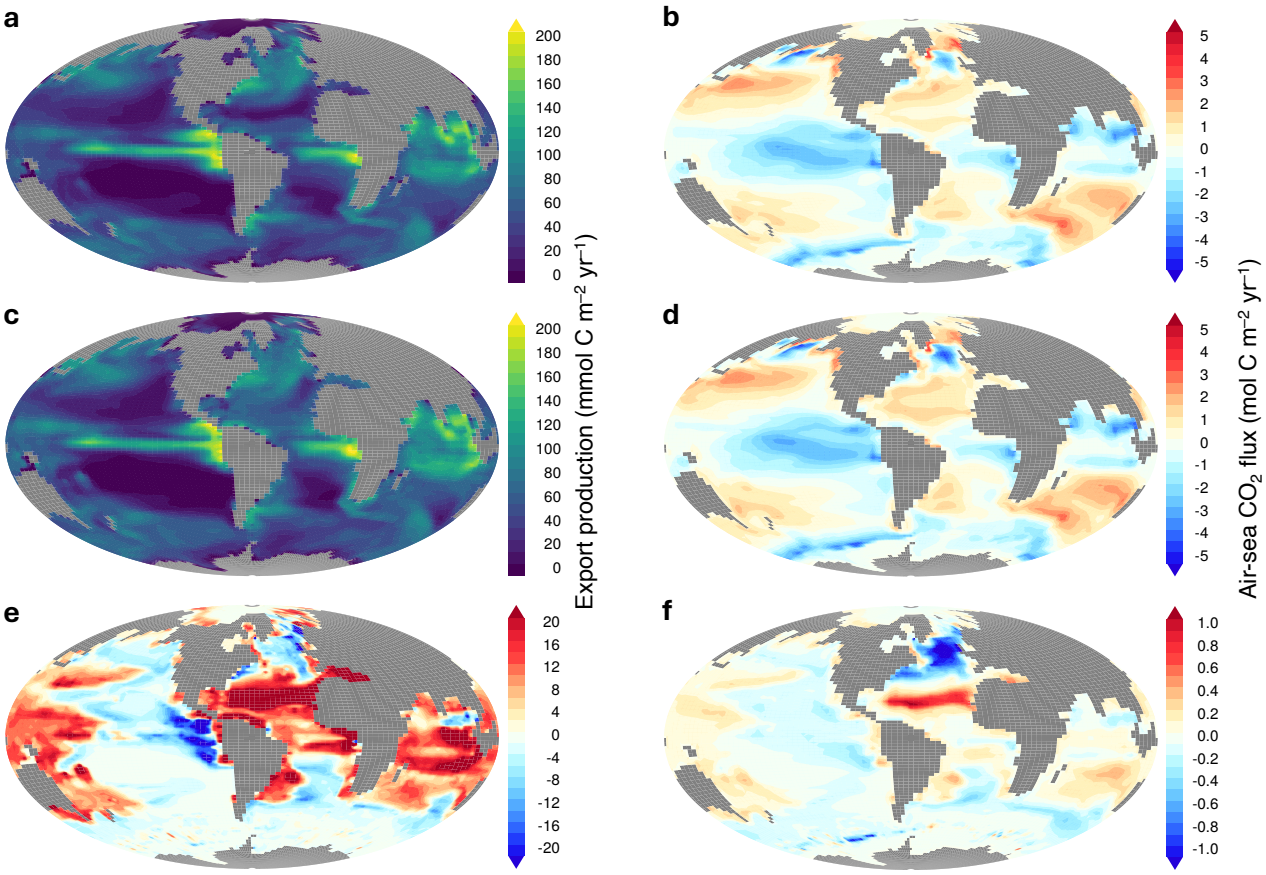

Figure 4. Export production at 130 m and air-sea carbon fluxes (positive downwards) at year 20k. a, b, V-CTL. c, d, V-P×2. e, f, V-P×2 − V-CTL.

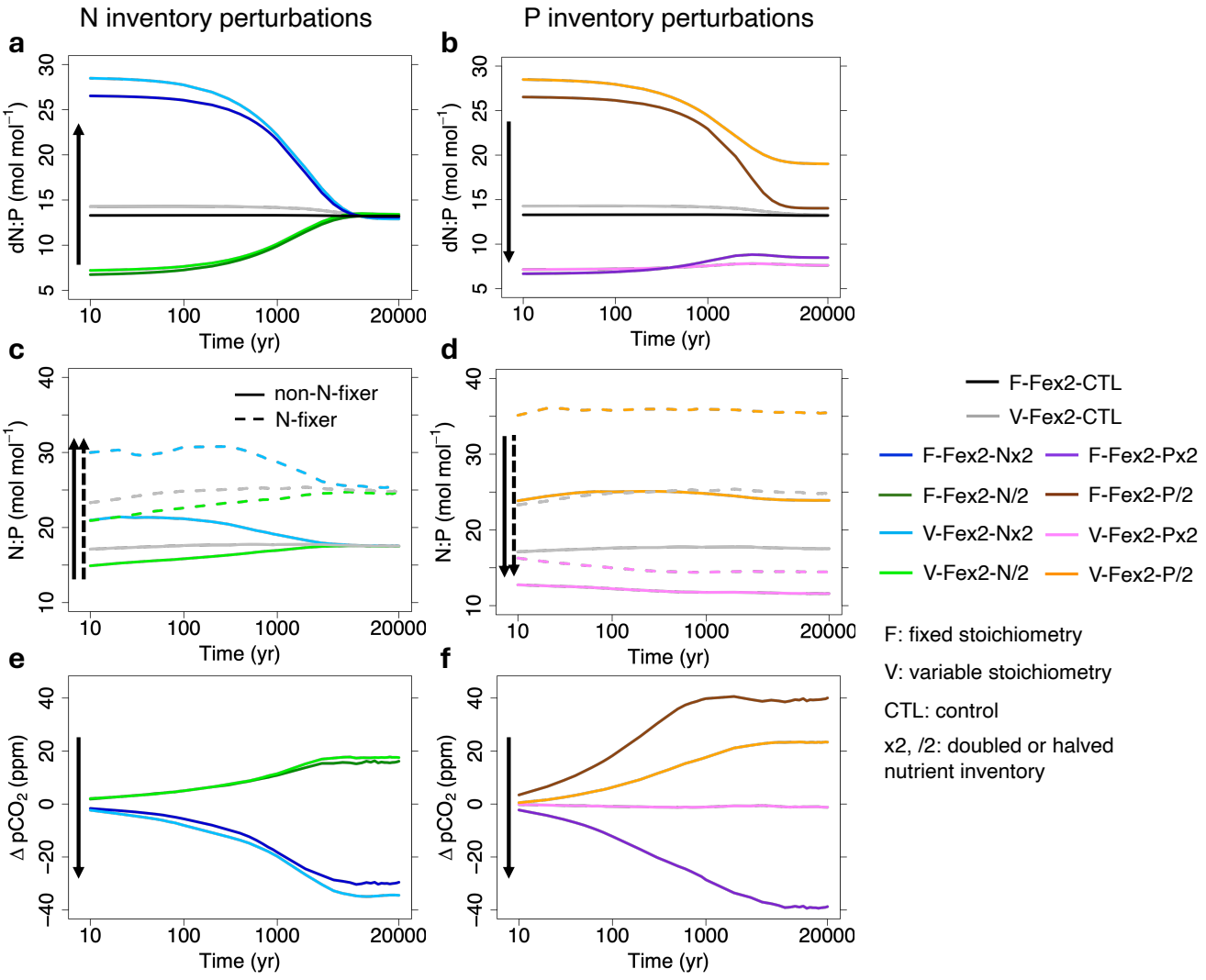

Figure 5. Temporal evolution of marine nutrient stoichiometry and atmospheric CO_2 in fixed- (FS) and variable-stoichiometry (VS) configurations with doubled Fe deposition (Fe×2) following NO_3^- or PO_4^{3-} inventory perturbations. **a, b,** Globally averaged dissolved nitrogen to phosphorus ratios (dN:P). **c, d,** N:P ratio shifts in non-N_2-fixers (solid lines) and N_2-fixers (dashed lines). **e, f,** Trajectories of atmospheric CO_2 concentration anomalies relative to the baseline controls. Black and grey lines represent the FS and VS control simulations, respectively. Vertical arrows indicate the direction of increasing initial nutrient inventories (from halved to doubled) relative to control baselines.

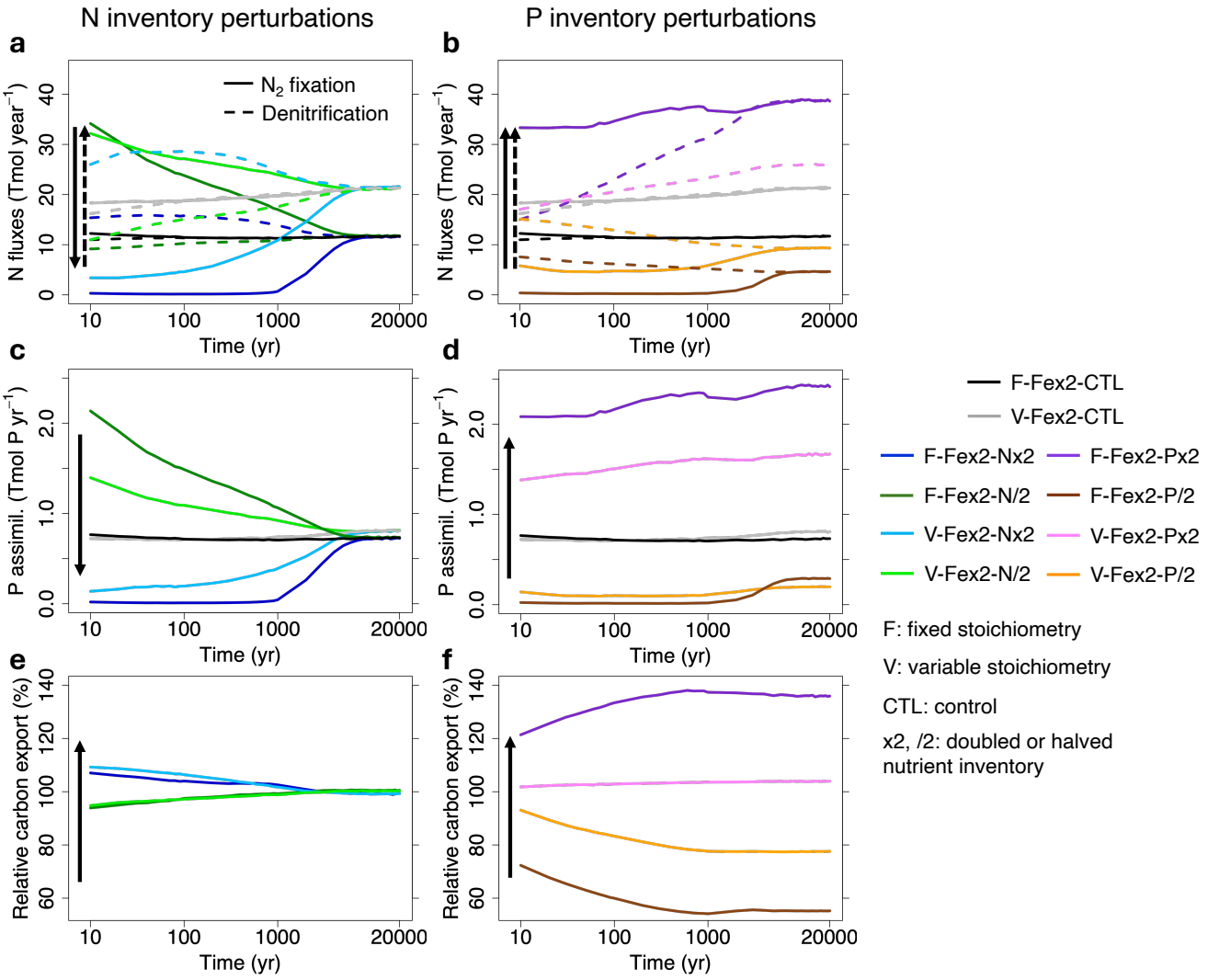

Figure 6. Temporal evolution of nitrogen fluxes, P assimilation, and POC export in fixed- (FS) and variable-stoichiometry (VS) configurations with doubled Fe deposition (Fe×2) following NO_3^- or PO_4^{3-} inventory perturbations. **a, b,** Global N_2 fixation (solid lines) and denitrification (water-column and benthic denitrification, dashed lines). **c, d,** Global phosphorus assimilation by N_2-fixers. **e, f,** Trajectories of global carbon export anomalies relative to the baseline controls. Black and grey lines represent the FS and VS control simulations, respectively. Vertical arrows indicate the direction of increasing initial nutrient inventories (from halved to doubled) relative to control baselines.

Table 1. Globally-averaged surface ocean temperature, AMOC at 26.5°N, NO_3^- concentrations, nitrogen to phosphorus ratios of dissolved and particulate organic matter (dN:P and pN:P, respectively) in the experiments at year 20k.

Configuration	Experiment	Surface temperature	AMOC 26.5°N	NO_3^-	dN:P	pN:P
		°C	Sv	mmol N m^{-3}	mol mol^{-1}	
VS	V-CTL	17.9	18.9	30.5	14.1	16.5
	V-N/2	18.1	19.2	30.5	14.1	16.5
	V-N×2	17.4	18.4	30.3	14.0	16.5
	V-P/2	18.0	19.2	20.7	19.1	21.9
	V-P×2	17.9	19.0	34.8	8.0	12.3
	V-Fe×2-CTL	17.6	18.5	28.8	13.3	17.3
	V-Fe×2-N/2	17.9	19.0	29.1	13.4	17.3
	V-Fe×2-N×2	17.1	18.0	28.0	12.9	17.3
	V-Fe×2-P/2	18.0	19.1	20.6	19.0	22.3
	V-Fe×2-P×2	17.6	18.5	33.0	7.6	12.5
FS	F-CTL	17.9	19.0	28.7	13.2	16
	F-N/2	18.1	19.2	28.8	13.3	16
	F-N×2	17.4	18.5	28.5	13.1	16
	F-P/2	18.3	19.4	15.2	14.0	16
	F-P×2	17.5	18.5	39.4	9.1	16
	F-Fe×2-CTL	17.8	18.3	28.6	13.2	16
	F-Fe×2-N/2	18.0	19.2	28.7	13.3	16
	F-Fe×2-N×2	17.4	18.2	28.4	13.1	16
	F-Fe×2-P/2	18.3	19.4	15.2	14.0	16
	F-Fe×2-P×2	17.2	18.1	36.8	8.5	16

Table 2. Global NO_3^- concentration, N_2 fixation, global non-N-fixers and N-fixers P assimilation, N:P ratio of N-fixers, and carbon export at 130 m at 10th year of the control simulations with VS and FS configurations.

Configuration	NO_3^-	N_2 fixation	non-N-fixers P assimilation	N-fixers P assimilation	N-fixers N:P	Carbon export
	$mmol\,m^{-3}$	$Tmol\,year^{-1}$			$mol\,mol^{-1}$	$Pg\,year^{-1}$
VS	30.9	15.1	50.8	0.61	23.1	9.6
FS	28.8	10.7	52.6	0.67	16.0	8.0

Table 3. Symbols used in the derivation of the fixed-stoichiometry (FS) configuration from the original variable-stoichiometry (VS) configuration of UVic-OPEM.

Symbol		Units	Description
VS	FS		
A_0		$\mathrm{m^3 mmol^{-1} d^{-1}}$	nutrient affinity for DIN and DIP
$\mathcal{B}$		—	shorthand for notational convenience
C		$\mathrm{mmol\,m^{-3}}$	phytoplankton particulate organic carbon concentration
${}^{\mathrm{VS}}\widehat{F}^{\mathrm{N}}$	${}^{\mathrm{FS}}\widehat{F}^{\mathrm{N}}$	$\mathrm{mol\,mol\,C^{-1} d^{-1}}$	potential specific N_2 fixation rate
F_0^{N}		$\mathrm{mol\,mol\,C^{-1} d^{-1}}$	maximum N_2 fixation rate of the N_2-fixation compartment
${}^{\mathrm{VS}}f_{\mathrm{C}}$	${}^{\mathrm{FS}}f_{\mathrm{C}}$	—	optimal allocation for C fixation
${}^{\mathrm{VS}}f_{\mathrm{N}}$	${}^{\mathrm{FS}}f_{\mathrm{N}}$	—	optimal allocation for DIN uptake or N_2 fixation within the nutrient-acquisition compartment
${}^{\mathrm{VS}}f_{\mathrm{V}}$	${}^{\mathrm{FS}}f_{\mathrm{V}}$	—	optimal allocation for nutrient acquisition
Q^{N}		$\mathrm{mol\,mol^{-1}}$	phytoplankton N quota (pN:C ratio)
Q_0^{N}		$\mathrm{mol\,mol^{-1}}$	phytoplankton minimum (subsistence) N quota (pN:C ratio)
$Q_{\mathrm{s}}^{\mathrm{N}}$		$\mathrm{mol\,mol^{-1}}$	phytoplankton non-allocatable partial N quota for structural protein
Q^{P}		$\mathrm{mol\,mol^{-1}}$	phytoplankton P quota (pP:C ratio)
Q_0^{P}		$\mathrm{mol\,mol^{-1}}$	phytoplankton minimum (subsistence) P quota (pP:C ratio)
V_0		$\mathrm{mol\,mol\,C^{-1} d^{-1}}$	maximum (temperature-dependent) turnover rate
${}^{\mathrm{VS}}V^{\mathrm{C}}$	${}^{\mathrm{FS}}V^{\mathrm{C}}$	$\mathrm{mmol\,m^{-3} d^{-1}}$	absolute C fixation rate
$\widehat{V}^{\mathrm{C}}$		$\mathrm{mol\,mol\,C^{-1} d^{-1}}$	potential specific C fixation rate
${}^{\mathrm{VS}}V^{\mathrm{N}}$	${}^{\mathrm{FS}}V^{\mathrm{N}}$	$\mathrm{mmol\,m^{-3} d^{-1}}$	absolute N uptake rate
${}^{\mathrm{VS}}\widehat{V}^{\mathrm{N}}$	${}^{\mathrm{FS}}\widehat{V}^{\mathrm{N}}$	$\mathrm{mol\,mol\,C^{-1} d^{-1}}$	potential specific N uptake rate
${}^{\mathrm{VS}}V_{\mathrm{max}}^{\mathrm{N}}$	${}^{\mathrm{FS}}V_{\mathrm{max}}^{\mathrm{N}}$	$\mathrm{mol\,mol\,C^{-1} d^{-1}}$	maximum (P-dependent) N assimilation rate of the nutrient-acquisition compartment
	${}^{\mathrm{FS}}\widetilde{V}^{\mathrm{N}}$	$\mathrm{mol\,mol\,C^{-1} d^{-1}}$	plug-in replacement for V^{N} for the calculation of ${}^{\mathrm{FS}}\widehat{V}^{\mathrm{N}}$
	${}^{\mathrm{FS}}\widetilde{V}_{\mathrm{max}}^{\mathrm{N}}$	$\mathrm{mol\,mol\,C^{-1} d^{-1}}$	plug-in replacement for $V_{\mathrm{max}}^{\mathrm{N}}$ for the calculation of ${}^{\mathrm{FS}}V_{\mathrm{max}}^{\mathrm{N}}$
${}^{\mathrm{VS}}V^{\mathrm{P}}$	${}^{\mathrm{FS}}V^{\mathrm{P}}$	$\mathrm{mmol\,m^{-3} d^{-1}}$	absolute P uptake rate
$\widehat{V}^{\mathrm{P}}$		$\mathrm{mol\,mol\,C^{-1} d^{-1}}$	potential specific P uptake rate
ζ^{N}		$\mathrm{mol\,mol\,N^{-1}}$	cost of N assimilation

Supplementary Discussion

Fixed versus flexible ecological stoichiometry

Anthropogenic inputs of bioavailable nitrogen are already substantially enhancing nitrogen availability even in the open ocean [35, 36, 37], with expected yet uncertain impacts on carbon fixation and radiative forcing within the atmosphere [35]. Previous studies assuming fixed stoichiometry for phytoplankton have found that enhanced denitrification and reduced nitrogen fixation operate as negative feedbacks, which limit the enhancement of global NPP by anthropogenic nitrogen supply in both an Earth system model [38] and an ocean biogeochemical model [39]. However, a recent study, also assuming fixed composition for both N-fixing and non-N-fixing phytoplankton in an Earth system model, found that anthropogenic sources of nitrogen (from both riverine inputs and atmospheric deposition) substantially enhanced modelled oceanic net primary production, which counteracts the effect of ocean stratification under future projections of global climate change [40]. Our results demonstrate that, compared to the assumption of fixed composition, accounting for the variable stoichiometry of phytoplankton substantially alters the response to enhanced nutrient supply over timescales from centuries to millennia. Most notably, in our variable-stoichiometry model, enhanced nitrogen supply results in substantially greater enhancement of denitrification and slightly greater oceanic uptake of CO_2 via a biogeochemical feedback qualitatively similar to that identified previously [41, 38, 39]. However, compared to our fixed-stoichiometry control model and to previous results [38], we find that variable stoichiometry for phytoplankton stabilises the system overall with respect to perturbations in nutrient supply, resulting in substantially smaller changes in N fixation rates and total nitrogen content.

Role of Fe supply

Fe is an essential element for photosynthesis and N_2 fixation, and its scarcity can impede the regulation of global dN:P [42, 43]. Alleviating Fe limitation could foster N_2 fixation [43], so that N_2-fixers could consume excess PO_4^{3-} and restore dN:P to its original value. This is also the premise for the direct proportionality of primary production to riverine input of P in [1]. Indeed, both P assimilation and N_2 fixation increase when the Fe supply doubles (Fig. 2b,d and Extended data Fig. 6b,d), and this also leads to higher carbon export for P×2 simulations (Fig. 2f and Extended data Fig. 6f).

Alleviation of Fe limitation on N_2 fixation is expected to increase NO_3^- input and facilitate the restoration of dN:P to their original values in the P×2 simulations. However, our results deviate from this expectation, and $[NO_3^-]$ even decreases in simulations with doubled Fe deposition, resulting in lower dN:P in both FS and VS configurations (Extended data Table 1).

On the one hand, doubling Fe deposition increases N_2 fixation in both the FS and VS configurations (Fig. 2a and Extended data Fig. 6a). On the other hand, the higher Fe supply also promotes the growth of non-N_2-fixers, enhancing ocean productivity and denitrification in general [24]. This increased NO_3^- loss through denitrification offsets the additional input from N_2 fixation. At equilibrium, Fe supply has a limited effect on dN:P (Extended data Table 1). Consequently, the strong stabilising effect of variable stoichiometry on the NO_3^- inventory appears to be largely insensitive to alleviation of Fe limitation.

The NO_3^- modification experiments yield a similar response. Both N_2 fixation and denitrification rates are enhanced by doubling Fe deposition, but the effects on dN:P, carbon export and ΔpCO_2 appear negligible at equilibrium (Fig. 1, Extended data Fig. 5).

Drivers of phytoplankton stoichiometry

The global relationship between pN:P and nutrient supply in the ocean has been attributed primarily to physiological plasticity (acclimation) by phytoplankton [4]. Compared to the assumption of fixed stoichiometry, flexible C:P of phytoplankton also implies a weaker relationship between preformed phosphate and atmospheric CO_2, as well as a more important role for the nitrogen cycle relative to the phosphorus cycle [4]. Hemispheric and regional variations in stoichiometry appear to be related to nutrient supply rate and nitrogen-versus-phosphorus stress for phytoplankton, with particulate C:N:P ratios largely determined by both nutrient supply and nutrient stress type (N or P) at low latitudes, based on an extensive global biogeochemical and genomic dataset [12]. In these data, pC:P and pN:P are positively correlated with the fraction of cyanobacteria and negatively with the fraction of diatoms in the observed phytoplankton communities, but community shifts alone can not explain inter-hemispheric differences in particulate stoichiometry [12]. Therefore, physiological acclimation, modulated by nitrogen or phosphorus limitation, also plays a major role in determining pN:P and pC:P. A strong positive correlation between observed N:P ratios of picocyanobacteria and picoeukaryotic phytoplankton and N:P supply ratios (to the near-surface ocean) has also been found across nutrient-rich and phosphorus-stressed biomes in the North Atlantic, but not in regions (such as the tropical North Pacific) where phytoplankton tend to be nitrogen stressed [44]. In this study, a combination of taxonomic composition and acclimation best predicted bulk particulate organic matter composition, supporting the idea that inter-specific differences in stoichiometry interact with intra-specific physiological acclimation to modulate phytoplankton stoichiometry and in turn the stoichiometry of bulk particles.

Recent results from mesocosm experiments using natural assemblages of plankton in the North Pacific subtropical gyre indicate that observed changes in pN:P generally reflect phytoplankton community composition, but that the full range of observed pN:P ratios, which varied substantially even for phytoplankton communities of similar composition, could not be explained without invoking acclimation as well [13]. Our results further demonstrate that acclimation could be the dominant factor for the variation in pN:P in the ocean.

Supplementary Methods

Derivation of the fixed-stoichiometry (FS) configuration of UVic-OPEM

The potential uptake rates of dissolved inorganic nitrogen (DIN = NO_3^-) and dissolved inorganic phosphorus (DIP = PO_4^{3-}) follow optimal uptake kinetics:

$$ {}^{\mathrm{VS}}\widehat{V}^{\mathrm{N}} = \left(\sqrt{\frac{1}{{}^{\mathrm{VS}}V^{\mathrm{N}}_{\max}}} + \sqrt{\frac{1}{A_0 \cdot [\mathrm{NO_3}^-]}} \right)^{-2}, \quad {}^{\mathrm{VS}}V^{\mathrm{N}}_{\max} = V_0 \cdot \left(1 - \frac{Q^{\mathrm{P}}_0}{Q^{\mathrm{P}}}\right) \quad \text{and} \quad \widehat{V}^{\mathrm{P}} = \left(\sqrt{\frac{1}{V_0}} + \sqrt{\frac{1}{A_0 \cdot [\mathrm{PO_4}^{3-}]}} \right)^{-2} \tag{9} $$

where the left-superscript $^{\mathrm{VS}}$ indicates variables specific to the original variable-stoichiometry (VS) configuration of UVic-OPEM and A_0 is nutrient affinity.

Growth rate (carbon fixation) is maximised via the optimality conditions

$$\frac{\mathrm{d}V^{\mathrm{C}}}{\mathrm{d}f_{\mathrm{V}}}=0 \quad \text{and} \quad \frac{\mathrm{d}(f_{\mathrm{N}}\cdot\widehat{V}^{\mathrm{N}})}{\mathrm{d}f_{\mathrm{N}}}=0 \quad \text{(DIN utilisation)} \quad \text{or} \quad \frac{\mathrm{d}(f_{\mathrm{N}}\cdot\widehat{F}^{\mathrm{N}})}{\mathrm{d}f_{\mathrm{N}}}=0 \quad (\mathrm{N_2}\text{ fixation}) \tag{10}$$

where the conditions for f_{N} follow from the chain-model assumption that $f_{\mathrm{N}}\cdot\widehat{V}^{\mathrm{N}}$ and $f_{\mathrm{N}}\cdot\widehat{F}^{\mathrm{N}}$ are regulated independently of V^{C} [28]. For the VS configuration, the optimality conditions are solved by [28]:

$$^{\mathrm{VS}}f_{\mathrm{V}}=\frac{Q^{\mathrm{N}}_{\mathrm{s}}}{Q^{\mathrm{N}}}-\zeta^{\mathrm{N}}\cdot(Q^{\mathrm{N}}-2\cdot Q^{\mathrm{N}}_{\mathrm{s}})=0.5\cdot\frac{Q^{\mathrm{N}}_0}{Q^{\mathrm{N}}}-\zeta^{\mathrm{N}}\cdot(Q^{\mathrm{N}}-Q^{\mathrm{N}}_0) \tag{11}$$

and

$$^{\mathrm{VS}}f_{\mathrm{N}}=\begin{cases}\dfrac{1}{1+\sqrt{\dfrac{Q^{\mathrm{P}}_0}{Q^{\mathrm{N}}}\cdot\dfrac{V_0}{\widehat{V}^{\mathrm{P}}}\cdot\left(\dfrac{^{\mathrm{VS}}\widehat{V}^{\mathrm{N}}}{^{\mathrm{VS}}V^{\mathrm{N}}_{\max}}\right)^{1.5}}}=\dfrac{1-\dfrac{Q^{\mathrm{P}}_0}{Q^{\mathrm{P}}}}{1-\dfrac{Q^{\mathrm{P}}_0}{Q^{\mathrm{P}}}\left(1-\sqrt{\dfrac{^{\mathrm{VS}}\widehat{V}^{\mathrm{N}}}{^{\mathrm{VS}}V^{\mathrm{N}}_{\max}}}\right)} & \text{for DIN utilisation}\\[2ex] \dfrac{1}{1+\sqrt{\dfrac{Q^{\mathrm{P}}_0}{Q^{\mathrm{N}}}\cdot\dfrac{F^{\mathrm{N}}_0}{\widehat{V}^{\mathrm{P}}}}}=1-\dfrac{Q^{\mathrm{P}}_0}{Q^{\mathrm{P}}} & \text{for } \mathrm{N_2}\text{ fixation}\end{cases} \tag{12}$$

where $Q^{\mathrm{N}}_0=2\cdot Q^{\mathrm{N}}_{\mathrm{s}}$ and Q^{P}_0 are the minimal (subsistence) N and P quotas and F^{N}_0 is the potential $\mathrm{N_2}$ fixation rate of the $\mathrm{N_2}$ fixation compartment. N-fixers are considered facultative diazotrophs, i.e., they switch between $\mathrm{N_2}$ fixation and DIN uptake, depending on environmental conditions [28, 29]. The two expressions each for DIN utilisation and $\mathrm{N_2}$ fixation in (12) are equivalent for balanced growth and the right-most terms are employed in the VS configuration.

The solution for $^{\mathrm{VS}}f_{\mathrm{N}}$ in (12) for DIN utilisation is based on the balanced-growth approximation

$$\frac{^{\mathrm{VS}}\widehat{V}^{\mathrm{N}}}{\widehat{V}^{\mathrm{P}}}=\left(\frac{1}{^{\mathrm{VS}}f_{\mathrm{N}}}-1\right)\cdot\frac{Q^{\mathrm{N}}}{Q^{\mathrm{P}}} \tag{13}$$

and the finding that [28]:

$$\frac{Q^{\mathrm{N}}}{Q^{\mathrm{P}}}\cdot\frac{\widehat{V}^{\mathrm{P}}}{^{\mathrm{VS}}\widehat{V}^{\mathrm{N}}}\cdot\mathcal{B}=1, \qquad \mathcal{B}=\frac{1}{\left(\dfrac{Q^{\mathrm{P}}}{Q^{\mathrm{P}}_0}-1\right)\cdot\sqrt{\dfrac{V_0}{^{\mathrm{VS}}\widehat{V}^{\mathrm{N}}}\cdot\left(1-\dfrac{Q^{\mathrm{P}}_0}{Q^{\mathrm{P}}}\right)}}=\frac{1}{\left(\dfrac{Q^{\mathrm{P}}}{Q^{\mathrm{P}}_0}-1\right)\cdot\sqrt{\dfrac{^{\mathrm{VS}}V^{\mathrm{N}}_{\max}}{^{\mathrm{VS}}\widehat{V}^{\mathrm{N}}}}} \tag{14}$$

The left expression for $^{\mathrm{VS}}f_{\mathrm{N}}$ in (12) for DIN utilisation is obtained by first solving (13) for $^{\mathrm{VS}}\widehat{V}^{\mathrm{N}}$, and then multiplying (14) with $^{\mathrm{VS}}\widehat{V}^{\mathrm{N}^2}\cdot Q^{\mathrm{P}}$:

$$\left(\frac{1}{^{\mathrm{VS}}f_{\mathrm{N}}}-1\right)^2\cdot\frac{Q^{\mathrm{N}}}{Q^{\mathrm{P}}}\cdot\frac{\widehat{V}^{\mathrm{P}}}{^{\mathrm{VS}}\widehat{V}^{\mathrm{N}}}=\mathcal{B} \tag{15}$$

and solving for ${}^{\mathrm{VS}}f_{\mathrm{N}}$. The right expression is found by rearranging (13) as $Q^{\mathrm{P}} \cdot {}^{\mathrm{VS}}\widehat{V}^{\mathrm{N}^2} = Q^{\mathrm{N}} \cdot (1/{}^{\mathrm{VS}}f_{\mathrm{N}} - 1) \cdot \widehat{V}^{\mathrm{P}} \cdot {}^{\mathrm{VS}}\widehat{V}^{\mathrm{N}}$, then again multiplying (14) with ${}^{\mathrm{VS}}\widehat{V}^{\mathrm{N}^2} \cdot Q^{\mathrm{P}}$:

$$\frac{1}{{}^{\mathrm{VS}}f_{\mathrm{N}}} - 1 = \mathcal{B} \tag{16}$$

The solution for ${}^{\mathrm{VS}}f_{\mathrm{N}}$ in (12) for N_2 fixation is derived from the balanced-growth approximation, analogously to (9) and (13):

$$\frac{{}^{\mathrm{VS}}\widehat{F}^{\mathrm{N}}}{\widehat{V}^{\mathrm{P}}} = \left(\frac{1}{{}^{\mathrm{VS}}f_{\mathrm{N}}} - 1\right) \cdot \frac{Q^{\mathrm{N}}}{Q^{\mathrm{P}}}, \qquad {}^{\mathrm{VS}}\widehat{F}^{\mathrm{N}} = F_0^{\mathrm{N}} \cdot \left(1 - \frac{Q_0^{\mathrm{P}}}{Q^{\mathrm{P}}}\right) \tag{17}$$

Eq. (17) is solved for Q^{P} and substituted into the right part of (17) to obtain ${}^{\mathrm{VS}}\widehat{F}^{\mathrm{N}}$ as a function of ${}^{\mathrm{VS}}f_{\mathrm{N}}$ and Q^{N}. Then, the optimality condition for f_{N} for N_2 fixation in (10) yields the left expression for ${}^{\mathrm{VS}}f_{\mathrm{N}}$ in (12) for N_2 fixation. The right expression follows from solving (17) for Q^{N} and substituting into the left expression.

For the FS configuration, the allocation factors f_{V} and f_{N} are calculated assuming balanced-growth approximations for constant Q^{N} and Q^{P}, based on the actual nitrogen and phosphorus uptake rates. However, maximal growth is achieved only as long as the fixed values for Q^{N} and Q^{P} happen to be close to the actual optimal values as determined by the allocation factors in the variable-stoichiometry configuration. Therefore, the constant Q^{N} and Q^{P} quotas are incompatible with truly optimal growth.

For DIN uptake, we first introduce ${}^{\mathrm{FS}}\widetilde{V}^{\mathrm{N}}_{\mathrm{max}}$ and ${}^{\mathrm{FS}}\widetilde{V}^{\mathrm{N}}$ as plug-in replacements for $V^{\mathrm{N}}_{\mathrm{max}}$ and $\widehat{V}^{\mathrm{N}}$ for fixed Q^{P}:

$${}^{\mathrm{FS}}\widetilde{V}^{\mathrm{N}} = \left(\sqrt{\frac{1}{{}^{\mathrm{FS}}\widetilde{V}^{\mathrm{N}}_{\mathrm{max}}}} + \sqrt{\frac{1}{A_0 \cdot [\mathrm{NO_3^-}]}}\right)^{-2}, \qquad {}^{\mathrm{FS}}\widetilde{V}^{\mathrm{N}}_{\mathrm{max}} = \left(1 - \frac{Q_0^{\mathrm{P}}}{Q^{\mathrm{P}}}\right) \cdot V_0 \tag{18}$$

Then, $V^{\mathrm{N}}_{\mathrm{max}}$ is approximated for the FS configuration as ${}^{\mathrm{FS}}V^{\mathrm{N}}_{\mathrm{max}}$ by substituting $1 - Q_0^{\mathrm{P}}/Q^{\mathrm{P}}$ by its balanced-growth equivalent obtained from (12) for DIN utilisation, $V^{\mathrm{N}}_{\mathrm{max}}$ by ${}^{\mathrm{FS}}\widetilde{V}^{\mathrm{N}}_{\mathrm{max}}$, and $\widehat{V}^{\mathrm{N}}$ by ${}^{\mathrm{FS}}\widetilde{V}^{\mathrm{N}}$:

$${}^{\mathrm{FS}}\widehat{V}^{\mathrm{N}} = \left(\sqrt{\frac{1}{{}^{\mathrm{FS}}V^{\mathrm{N}}_{\mathrm{max}}}} + \sqrt{\frac{1}{A_0 \cdot [\mathrm{NO_3^-}]}}\right)^{-2}, \qquad {}^{\mathrm{FS}}V^{\mathrm{N}}_{\mathrm{max}} = \left(1 - \frac{Q_0^{\mathrm{P}}}{Q^{\mathrm{P}}}\right) \cdot V_0 \approx \frac{V_0}{1 + \sqrt{\frac{Q_0^{\mathrm{P}}}{Q^{\mathrm{N}}} \cdot \frac{V_0}{\widehat{V}^{\mathrm{P}}} \cdot \sqrt{\frac{{}^{\mathrm{FS}}\widetilde{V}^{\mathrm{N}}}{{}^{\mathrm{FS}}\widetilde{V}^{\mathrm{N}}_{\mathrm{max}}}}}} \tag{19}$$

For N_2 fixation, we substitute $1 - Q_0^{\mathrm{P}}/Q^{\mathrm{P}}$ with the balanced-growth approximation from (12) for N_2 fixation:

$${}^{\mathrm{FS}}\widehat{F}^{\mathrm{N}} = F_0^{\mathrm{N}} \cdot \left(1 - \frac{Q_0^{\mathrm{P}}}{Q^{\mathrm{P}}}\right) = \frac{F_0^{\mathrm{N}}}{1 + \sqrt{\frac{Q_0^{\mathrm{P}}}{Q^{\mathrm{N}}} \cdot \frac{F_0^{\mathrm{N}}}{\widehat{V}^{\mathrm{P}}}}} \tag{20}$$

Thus we obtain the allocation factor ${}^{\mathrm{FS}}f_{\mathrm{N}}$ for DIN uptake or N_2 fixation for the FS configuration:

$${}^{\mathrm{FS}}f_{\mathrm{N}} = \begin{cases} \dfrac{1}{1 + \sqrt{\dfrac{Q_0^{\mathrm{P}}}{Q^{\mathrm{N}}} \cdot \dfrac{V_0}{\widehat{V}^{\mathrm{P}}} \cdot \left(\dfrac{{}^{\mathrm{FS}}\widehat{V}^{\mathrm{N}}}{{}^{\mathrm{FS}}V^{\mathrm{N}}_{\mathrm{max}}}\right)^{1.5}}} & \text{for DIN utilisation} \\ \dfrac{1}{1 + \sqrt{\dfrac{Q_0^{\mathrm{P}}}{Q^{\mathrm{N}}} \cdot \dfrac{F_0^{\mathrm{N}}}{\widehat{V}^{\mathrm{P}}}}} & \text{for } N_2 \text{ fixation} \end{cases} \tag{21}$$

where Q_0^{P}, F_0^{N}, and $\widehat{V}^{\mathrm{P}}$ are subsistence P quota, potential N_2 fixation rate, and potential rate of P assimilation.

The allocation factor ${}^{\mathrm{FS}}f_{\mathrm{V}}$ for FS is then a function of the potential rates of (light-limited) carbon fixation, $\widehat{V}^{\mathrm{C}}$, and N acquisition, ${}^{\mathrm{FS}}f_{\mathrm{N}} \cdot ({}^{\mathrm{FS}}\widehat{V}^{\mathrm{N}} + {}^{\mathrm{FS}}\widehat{F}^{\mathrm{N}})$:

$$ {}^{\mathrm{FS}}f_{\mathrm{V}} = \frac{\widehat{V}^{\mathrm{C}} \cdot Q_{\mathrm{s}}^{\mathrm{N}}}{{}^{\mathrm{FS}}f_{\mathrm{N}} \cdot ({}^{\mathrm{FS}}\widehat{V}^{\mathrm{N}} + {}^{\mathrm{FS}}\widehat{F}^{\mathrm{N}})} \left[-1 + \sqrt{1 + \frac{1}{Q_{\mathrm{s}}^{\mathrm{N}} \cdot (\widehat{V}^{\mathrm{C}} / [{}^{\mathrm{FS}}f_{\mathrm{N}} \cdot ({}^{\mathrm{FS}}\widehat{V}^{\mathrm{N}} + {}^{\mathrm{FS}}\widehat{F}^{\mathrm{N}})] + \zeta^{\mathrm{N}})} } \right] \tag{22} $$

where ζ^{N} is the cost of N assimilation and $\widehat{V}^{\mathrm{C}}$ is the same for VS and FS because it does not depend on Q^{N} [28]. The FS approximation (${}^{\mathrm{FS}}f_{\mathrm{V}}$) in (22) is equivalent to ${}^{\mathrm{VS}}f_{\mathrm{V}}$ in (11) for instantaneous balanced growth with variable stoichiometry [28].

References

1. Tyrrell, T. The relative influences of nitrogen and phosphorus on oceanic primary production. *Nature* **400**, 525–531 (1999).

2. Gruber, N. The dynamics of the marine nitrogen cycle and its influence on atmospheric CO2 variations. In Follows, M. & Oguz, T. (eds.) *The Ocean Carbon Cycle and Climate*, 97–148 (Springer Netherlands, Dordrecht, 2004).

3. Martiny, A. C. *et al.* Strong latitudinal patterns in the elemental ratios of marine plankton and organic matter. *Nature Geosci.* **6**, 279–283 (2013).

4. Galbraith, E. D. & Martiny, A. C. A simple nutrient-dependence mechanism for predicting the stoichiometry of marine ecosystems. *Proc. Natl. Acad. Sci. USA* **112**, 8199–8204 (2015).

5. Inomura, K., Deutsch, C., Jahn, O., Dutkiewicz, S. & Follows, M. J. Global patterns in marine organic matter stoichiometry driven by phytoplankton ecophysiology. *Nature Geosci.* **15**, 1034–1040 (2022).

6. Paytan, A. & McLaughlin, K. The oceanic phosphorus cycle. *Chem. Rev.* **107**, 563–576 (2007).

7. Deutsch, C., Sarmiento, J. L., Sigman, D. M., Gruber, N. & Dunne, J. P. Spatial coupling of nitrogen inputs and losses in the ocean. *Nature* **445**, 163–167 (2007).

8. Lenton, T. M. & Klausmeier, C. A. Biotic stoichiometric controls on the deep ocean n:p ratio. *Biogeosciences* **4**, 353–367 (2007).

9. Redfield, A. *On the proportions of organic derivatives in seawater and their relation to the composition of plankton.*, 177–192 (University Press of Liverpool, 1934).

10. Redfield, A. C. The biological control of chemical factors in the environment. *American Scientist* **46**, 205–221 (1958).

11. Lenton, T. M. & Watson, A. J. Redfield revisited 1. regulation of nitrate, phosphate, and oxygen in the ocean. *Glob. Biogeochem. Cycles* **14** (2001).

12. Tanioka, T. *et al.* Global patterns and predictors of c:n:p in marine ecosystems. *Commun. Earth Environ.* **3**, 271 (2022).

13. Seelen, E. A. *et al.* Nitrogen and phosphorus differentially control marine biomass production and stoichiometry. *Nat. Commun.* **16**, 5713 (2025).

14. Weber, T. & Deutsch, C. Oceanic nitrogen reservoir regulated by plankton diversity and ocean circulation. *Nature* **489**, 419–422 (2012).

15. Fu, F.-X., Zhang, Y., Bell, P. R. F. & Hutchins, D. A. Phosphate uptake and growth kinetics of *Trichodesmium* (cyanobacteria) isolates from the north Atlantic Ocean and the Great Barrier Reef, Australia. *Journal of Phycology* **41**, 62–73 (2005).

16. Fu, F. *et al.* Differing responses of marine N2 fixers to warming and consequences for future diazotroph community structure. *Aquatic Microbial Ecology* **72**, 33–46 (2014).

17. Knapp, A. N., Dekaezemacker, J., Bonnet, S., Sohm, J. A. & Capone, D. G. Sensitivity of *Trichodesmium erythraeum* and *Crocosphaera watsonii* abundance and N2 fixation rates to varying NO3 and PO4 concentrations in batch cultures. *Aquatic Microbial Ecology* **66**, 223–236 (2012).

18. Krauk, J., Villareal, T., Sohm, J., Montoya, J. & Capone, D. Plasticity of N:P ratios in laboratory and field populations of *Trichodesmium* spp. *Aquatic Microbial Ecology* **42**, 243–253 (2006).

19. Qu, P. *et al.* Distinct responses of the nitrogen-fixing marine cyanobacterium *Trichodesmium* to a thermally variable environment as a function of phosphorus availability. *Frontiers in Microbiology* **Volume 10** (2019).

20. Tuo, S.-h., Hu, Y.-Y., Irwin, A. J., Follows, M. J. & Finkel, Z. V. Phosphate modulates elemental and macromolecular composition of unicellular nitrogen-fixing cyanobacteria. *Limnology and Oceanography* **71**, e70475 (2026).

21. Zhu, Z. *et al.* Interactions between ultraviolet radiation exposure and phosphorus limitation in the marine nitrogen-fixing cyanobacteria *Trichodesmium* and *Crocosphaera*. *Limnology and Oceanography* **65**, 363–376 (2020).

22. Bopp, L. *et al.* Diazotrophy as a key driver of the response of marine net primary productivity to climate change. *Biogeosciences* **19**, 4267–4285 (2022).

23. Wu, J. *et al.* Dissolved inorganic phosphorus, dissolved iron, and *Trichodesmium* in the oligotrophic South China Sea. *Global Biogeochem. Cycles* **17** (2003).

24. Martin, J. H. & Fitzwater, S. E. Iron deficiency limits phytoplankton growth in the north-east Pacific subarctic. *Nature* **331**, 341–343 (1988).

25. Tanioka, T. & Matsumoto, K. A meta-analysis on environmental drivers of marine phytoplankton C : N : P. *Biogeosciences* **17**, 2939–2954 (2020).

26. Wang, W.-L., Moore, J. K., Martiny, A. C. & Primeau, F. W. Convergent estimates of marine nitrogen fixation. *Nature* **566**, 205–211 (2019).

27. Paerl, H. W. Why does N-limitation persist in the world's marine waters? *Marine Chemistry* **206**, 1–6 (2018).

28. Pahlow, M., Dietze, H. & Oschlies, A. Optimality-based model of phytoplankton growth and diazotrophy. *Marine Ecology Progress Series* **489**, 1–16 (2013).

29. Pahlow, M., Chien, C.-T., Arteaga, L. A. & Oschlies, A. Optimality-based non-redfield plankton–ecosystem model (opem v1.1) in uvic-escm 2.9 – part 1: Implementation and model behaviour. *Geosci. Model Dev.* **13**, 4663–4690 (2020).

30. Chien, C.-T., Pahlow, M., Schartau, M. & Oschlies, A. Optimality-based non-redfield plankton–ecosystem model (opem v1.1) in uvic-escm 2.9 – part 2: Sensitivity analysis and model calibration. *Geosci. Model Dev.* **13**, 4691–4712 (2020).

31. Auguères, A. & Loreau, M. Regulation of Redfield ratios in the deep ocean. *Global Biogeochem. Cycles* **29**, 254–266 (2015).

32. Chien, C.-T., Pahlow, M., Schartau, M., Li, N. & Oschlies, A. Effects of phytoplankton physiology on global ocean biogeochemistry and climate. *Science Advances* **9**, eadg1725 (2023).

33. Tanioka, T. *et al.* Global ocean particulate organic phosphorus, carbon, oxygen for respiration, and nitrogen (go-popcorn). *Scientific Data* **9**, 688 (2022).

34. Sharoni, S. & Halevy, I. Nutrient ratios in marine particulate organic matter are predicted by the population structure of well-adapted phytoplankton. *Science Advances* **6** (2020).

35. Duce, R. A. *et al.* Impacts of atmospheric anthropogenic nitrogen on the open ocean. *Science* **320**, 893–897 (2008).

36. Meng, Y. *et al.* Impacts of decadal increasing nitrogen deposition on North Pacific marine ecosystems. *J. Environ. Manag.* **379**, 124844 (2025).

37. Taketani, F., Matsumoto, K., Sekiya, T., Yamaji, K. & Kanaya, Y. An observational case study for inorganic nitrogen dry deposition potential on sea-surface primary production in the subtropical, western North Pacific. *Scientific Reports* **16**, 9068 (2026).

38. Yang, S. & Gruber, N. The anthropogenic perturbation of the marine nitrogen cycle by atmospheric deposition: Nitrogen cycle feedbacks and the 15N haber-bosch effect. *Global Biogeochem. Cycles* **30**, 1418–1440 (2016).

39. Somes, C. J., Landolfi, A., Koeve, W. & Oschlies, A. Limited impact of atmospheric nitrogen deposition on marine productivity due to biogeochemical feedbacks in a global ocean model. *Geophys. Res. Lett.* **43**, 4500–4509 (2016).

40. Yamamoto, A. *et al.* Competing and accelerating effects of anthropogenic nutrient inputs on climate-driven changes in ocean carbon and oxygen cycles. *Science Advances* **8**, eabl9207 (2022).

41. Landolfi, A., Dietze, H., Koeve, W. & Oschlies, A. Overlooked runaway feedback in the marine nitrogen cycle: the vicious cycle. *Biogeosciences* **10**, 1351–1363 (2013).

42. Falkowski, P. G. Evolution of the nitrogen cycle and its influence on the biological sequestration of CO2 in the ocean. *Nature* **387**, 272–275 (1997).

43. Moore, J. K. & Doney, S. C. Iron availability limits the ocean nitrogen inventory stabilizing feedbacks between marine denitrification and nitrogen fixation. *Global Biogeochem. Cycles* **21** (2007).

44. Lomas, M. W. *et al.* Varying influence of phytoplankton biodiversity and stoichiometric plasticity on bulk particulate stoichiometry across ocean basins. *Commun. Earth Environ.* **2**, 143 (2021).